nature microbiology

LETTERS

https://doi.org/10.1038/s41564-019-0378-9

Pseudomonas aeruginosa orchestrates twitching motility by sequential control of type IV pili movements

Lorenzo Talà[1], Adam Fineberg[2], Philipp Kukura[2] and Alexandre Persat[1*]

Prokaryotes have the ability to walk on surfaces using type IV pili (TFP), a motility mechanism known as twitching[1,2]. Molecular motors drive TFP extension and retraction, but whether and how these movements are coordinated is unknown[3]. Here, we reveal how the pathogen *Pseudomonas aeruginosa* coordinates the motorized activity of TFP to power efficient surface motility. To do this, we dynamically visualized TFP extension, attachment and retraction events at high resolution in four dimensions using label-free interferometric scattering microscopy (iSCAT)[4]. By measuring TFP dynamics, we found that the retraction motor PilT was sufficient to generate tension and power motility in free solution, while its partner ATPase PilU may improve retraction only in high-friction environments. Using precise timing of successive attachment and retraction, we show that *P. aeruginosa* engages PilT motors very rapidly and almost only when TFP encounter the surface, suggesting contact sensing. Finally, measurements of TFP dwell times on surfaces show that tension reinforced the adhesion strength to the surface of individual pili, thereby increasing effective pulling time during retraction. The successive control of TFP extension, attachment, retraction and detachment suggests that sequential control of motility machinery is a conserved strategy for optimized locomotion across domains of life.

Protein filaments decorate the surface of prokaryotes, allowing single cells to physically interact with their surroundings through motility, adhesion, gene exchange and signaling[5,6]. For example, *P. aeruginosa* performs successive rounds of motor-driven TFP extension and retraction to power twitching motility and regulate virulence through mechano-sensing[7–9]. Pili retraction motors can generate up to 100 pN, but how such large forces can power cell body displacements remains unclear[10,11]. To answer this question, the distribution of individual pili around single cells has been indirectly inferred from tracking of cell body displacements[12]. Also, labeling strategies have largely helped in the visualization of extension and retraction events, but also in deciphering the function of TFP in horizontal gene transfer and mechano-sensing[13,14]. These methods are powerful but remain invasive, and are limited by labeling robustness during high-speed or long-term imaging of TFP. As a result, changes in TFP length, number and extension–retraction frequencies, which ultimately regulate bacterial interaction with the environment, are difficult to measure during the course of motility. Understanding this connection therefore rests on our ability to visualize and monitor the dynamics of individual TFP on short timescales of extension–retraction (subseconds) and on longer timescales of surface colonization (minutes to hours).

To explore the coordination of their movements, we sought to directly image successive TFP extension–retraction events. iSCAT has previously been used to image single actin filaments in vitro without labels[15]. We reasoned that since actin and TFP are both protein polymers with an approximate width of 5 nm, iSCAT might enable TFP visualization. To achieve this, we adapted iSCAT to live-cell imaging (Supplementary Fig. 1)[16]. We reduced phototoxicity by using less energetic iSCAT and autofocus laser lines, and reduced unnecessary illumination by adding a shutter in the iSCAT illumination path with a brightfield channel for initial bacterial detection (see Methods).

Under brightfield illumination, wild-type *P. aeruginosa* appeared to be rod-shaped with no visible surface structures (Fig. 1a, left panel). Simultaneous iSCAT images of the same cell revealed micrometer-long extracellular filaments and shorter structures with alternating intensity extending from the cell body (Fig. 1a, right panel). Cells of in-frame deletion mutants in the pilin subunit gene *pilA* displayed no such slender structures (Fig. 1b), suggesting these were TFP. A deletion of the flagellin gene *fliC* removed structures with periodic pattern (Fig. 1c and Supplementary Fig. 2), suggesting that this signal was generated by a single helical flagellum with a periodicity of 1.4 ± 0.1 µm (s.e.m., $n = 10$), consistent with previous measurements for helical pitch[17]. Quantification of filaments showed that the wild-type cells had approximately one pilus per cell, *pilA*$^-$ had no TFP and *fliC*$^-$ had about five (Fig. 1d, Supplementary Fig. 2 and Methods) and that, as expected, most wild-type cells had one flagellum and *fliC*$^-$ had zero (Supplementary Fig. 2).

Live-cell iSCAT can capture multiple successive extension–retraction events while monitoring cell body displacements. For example, Supplementary Video 1 shows a one-minute visualization of a wild-type cell exhibiting multiple rounds of TFP attachment and retraction. Such sequences allow us to quantify attachment–retraction frequencies while monitoring cell body displacement (Supplementary Fig. 3). Since the signal generated from the flagellum was stronger than that from TFP, and because swimming may interfere with twitching motility, we sought to perform most dynamic visualizations on a *fliC*$^-$ background. We tested whether this would affect TFP dynamics, and found that there were no distinguishable differences in either cell displacement per retraction or retraction frequencies between wild-type cells and the flagellum-less mutant (Supplementary Fig. 4 and Supplementary Videos 1 and 2).

We observed three distinct patterns generated by TFP on iSCAT images: straight dark filaments, straight filaments with alternating black and white contrast and curved filaments with fainter contrast

[1]Institute of Bioengineering and Global Health Institute, School of Life Sciences, École Polytechnique Fédérale de Lausanne, Lausanne, Switzerland. [2]Department of Chemistry, Physical and Theoretical Chemistry Laboratory, University of Oxford, Oxford, UK. *e-mail: alexandre.persat@epfl.ch

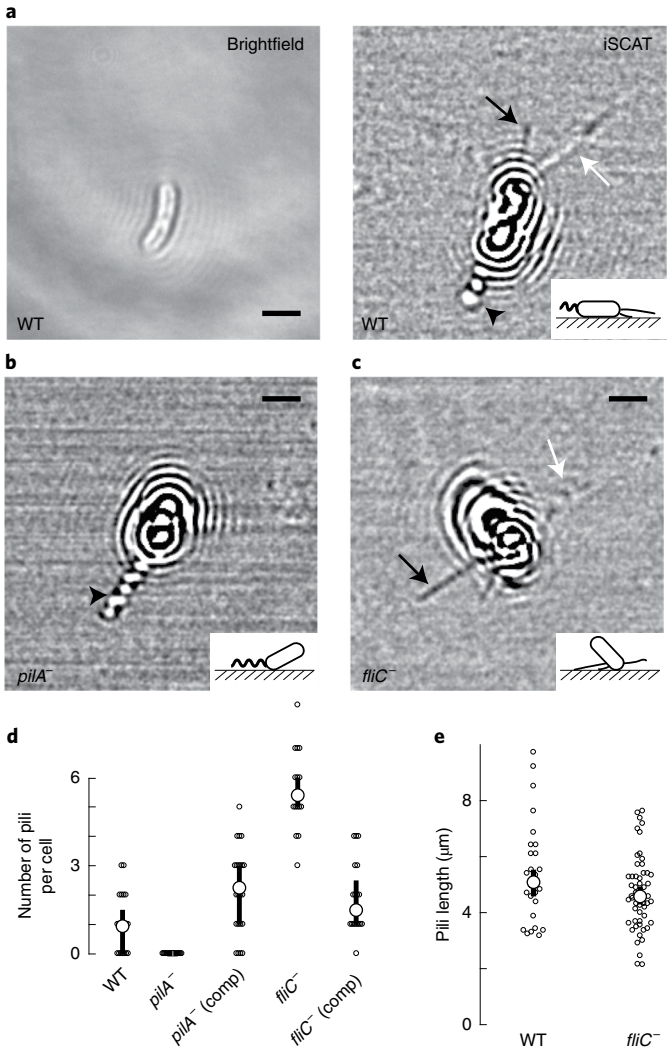

Fig. 1 | iSCAT reveals extracellular bacterial filaments. a, Brightfield (left) and iSCAT (right) images of a single wild-type (WT) *P. aeruginosa* cell. The brightfield image shows only the rod-shaped body of the bacterium, while multiple extracellular structures are visible in iSCAT. Flagellum (black arrowhead) and type IV pili with constant (black arrow) or spatially varying contrast (white arrow). **b**, A deletion mutant of the pilin gene *pilA* displayed no extracellular slender structures. **c**, A mutant in the flagellin subunit gene *fliC* had no polar filaments with alternating contrast. Inserted illustrations in iSCAT images show the position of cell and filaments relative to the coverslip surface. **d**, Quantification of mean TFP per cell with iSCAT. WT has about one pilus per cell on average (cells from the same culture $n=20$), *pilA* has none ($n=19$) but WT levels are restored in the complemented strain ($n=22$). *fliC*⁻ mutant cells have more TFP than WT ($n=15$), which decreases to WT level in the complemented strain ($n=18$). We attribute the hyperpiliation of *fliC*⁻ to a selection effect during sample loading (see Methods). Small circles are individual measurements, large circles are means of bootstrap medians and error bars represent bootstrap 95% confidence interval. **e**, Attached TFP length distribution in WT (combined number of pili from cells imaged in at least three biological replicates $n=27$) and *fliC*⁻ ($n=54$). The flagellum-less mutant has no defect in TFP length. Small circles represent individual measurements, large circles are bootstrap medians and error bars bootstrap 95% confidence interval. **a**–**c**, Scale bars, 2 μm.

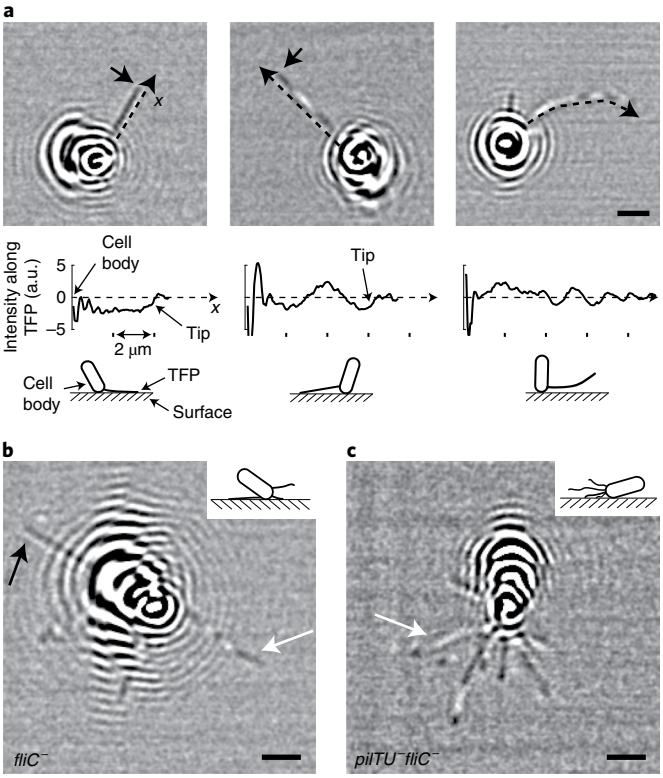

Fig. 2 | Visualization of TFP position and retraction in three dimensions. **a**, Images of three representative TFP positions and orientations visualized by iSCAT, with corresponding iSCAT intensity values along the length of the fibre (below). Changes in iSCAT contrast allow the inference of pilus position in three dimensions. TFP that have constant contrast lie flat on the surface (left panel), those with alternating contrast form a finite angle with the coverslip (middle panel), while curved fibres with oscillating and irregular contrast are defined as floppy (right panel). Below each image, a plot of the pixel gray value along the pilus allows determination of whether the pili lie flat, at an angle or are fluctuating. The illustration represents the putative three-dimensional orientation of the pilus and cell body. **b**, TFP of *fliC*⁻ deletion mutant cells exhibit all three morphologies (Supplementary Video 3). **c**, Cells lacking retraction motor genes *pilT* and *pilU* show only floppy TFP, demonstrating that retraction and tension force generates straight TFP morphology (Supplementary Video 4). We encountered these features throughout all our visualizations. Tensed (black arrows), floppy (white arrows), flat and angled pili were observed with similar results in all our retractile strains (WT, *fliC*⁻ and *pilU*⁻ *fliC*⁻), whereas only floppy pili were observed in our *pilT*⁻ *fliC*⁻. Scale bars, 2 μm. a.u., arbitrary units.

(Fig. 2a). Changes in the contrast of a fibre are a manifestation of the shift from constructive to destructive interference, with a full phase change corresponding to a spatial shift of $\lambda/2n$, where λ is the illumination wavelength and n the index of refraction of the medium[18].

Intensity values can thus be used as a proxy for in-depth position of TFP[19]. For example, TFP of uniform intensity lay flat against the surface (Fig. 2a, left panel). Those exhibiting successive positive and negative intensity values along their length are at an angle (Fig. 2a, middle and right panels). As a result, single iSCAT images provide us with the position and orientation of single TFP in three dimensions, thereby allowing quantitative inference of spatial position on and away from the attachment surface. We could, for example, observe differences in TFP positioning of standing versus horizontal cells[1]. TFP of standing cells, which orient vertically on the surface attached by one pole, were mostly (79%) flat against the surface, as shown in Fig. 2a. In contrast, in crawling horizontal cells, TFP were in most cases (81%) oriented at an angle between the glass surface and the cell pole (Fig. 1a). In summary, iSCAT provides the ability to probe TFP dynamics at high spatial and temporal resolution in three dimensions, without obstructing native biological functions.

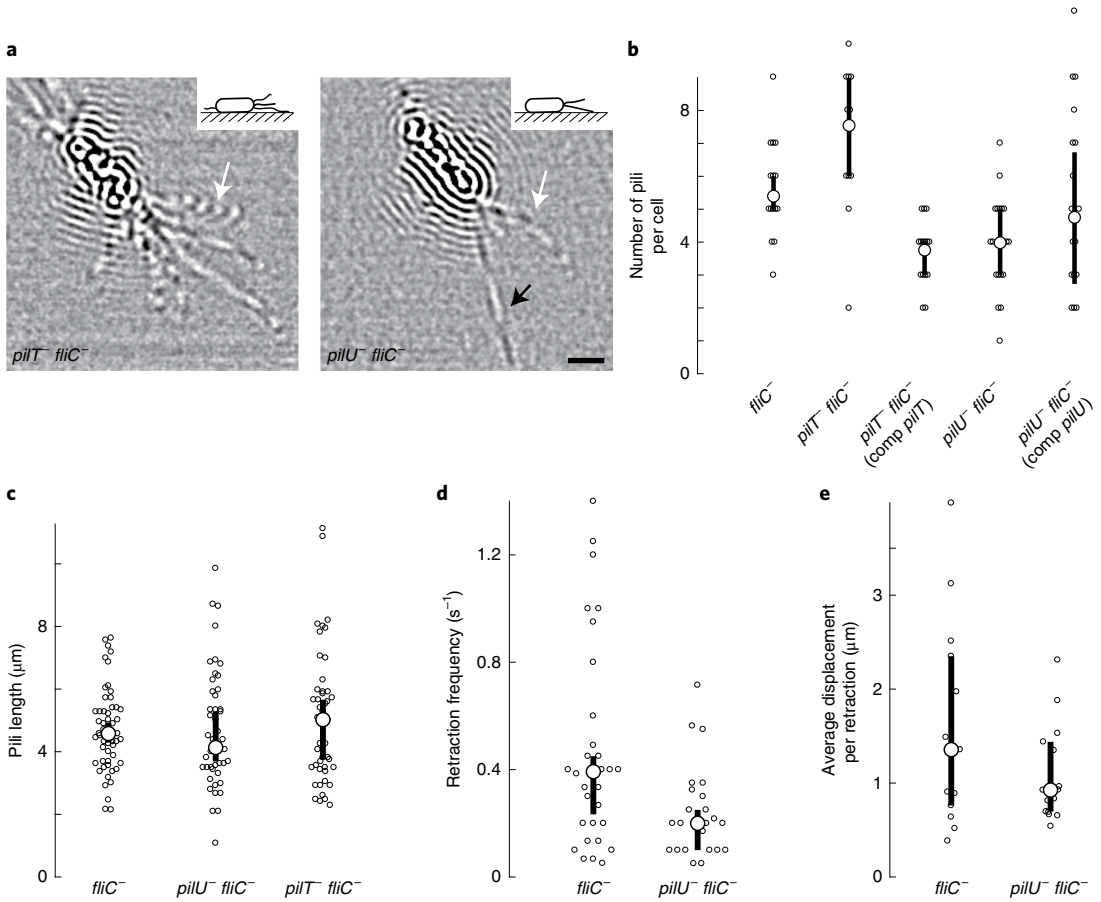

Fig. 3 | PilU does not affect TFP dynamics in free solution. a, iSCAT images of mutants *pilT*⁻ *fliC*⁻ and *pilU*⁻ *fliC*⁻. *pilT*⁻ *fliC*⁻ cells did not undergo retraction on the timescale of our movies. The *pilU*⁻ *fliC*⁻ mutant image shows retraction of one TFP. The black arrow indicates a tensed pilus; the white arrows indicate floppy pili. Scale bar, 2 μm. **b**, Number of TFP in motor mutants and their corresponding complementation strains. These have similar numbers of surface pili, except for *pilT*⁻ *fliC*⁻ (cells from the same culture, $n=11$), which had more (*fliC*⁻, $n=15$; *pilT*⁻ *fliC*⁻ complemented, $n=15$; *pilU*⁻ *fliC*⁻, $n=18$; *pilU*⁻ *fliC*⁻ complemented, $n=17$). Large circles are means of bootstrap medians and error bars are bootstrap 95% confidence intervals. Small circles are individual measurements. **c**, Average lengths of TFP that attached to the glass surface in *fliC*⁻ (combined number of pili from cells imaged in at least three biological replicates, $n=54$), *pilU*⁻ *fliC*⁻ ($n=47$) and *pilT*⁻ *fliC*⁻ ($n=45$). **d**, Retraction frequencies for *pilU*⁻ mutant (combined number of pili from cells imaged in at least three biological replicates, $n=23$) compared to *fliC*⁻ ($n=23$). The *pilU*⁻ mutant shows a slight decrease in retraction frequency compared to *fliC*⁻. **e**, Average displacement per retraction for *fliC*⁻ (number of tracks, $n=13$) and *pilU*⁻ *fliC*⁻ ($n=15$). Motility did not differ markedly among these mutants. **c**,**d**,**e**, Small circles correspond to individual measurements, large circles are medians of bootstrap medians and error bars are bootstrap 95% confidence interval. A difference between two groups is defined as statistically significant when their 95% confidence intervals do not overlap.

These images highlight two distinct TFP morphologies and dynamics: straight stationary and curved fluctuating filaments. We verified that the straight conformation was a result of tension generated during retraction. At the molecular level, the extension motor PilB polymerizes PilA subunits to drive TFP growth. The two retraction motors, PilT and PilU, drive retraction by depolymerizing PilA back into the periplasm, but whether their functions are redundant remains unclear[7,20]. *fliC*⁻ cells displayed both fluctuating curved and stationary straight TFP (Fig. 2b and Supplementary Video 3). In contrast, a *pilTU*⁻ *fliC*⁻ mutant had only curved TFP that were fluctuating (Fig. 2c and Supplementary Video 4). This demonstrates that straight TFP are under tension during retraction.

Given the lack of a clear function for the two retraction motors in *P. aeruginosa*, we sought to identify functional differences between PilT and PilU by visualizing TFP dynamics in respective mutants. Both *pilT* and *pilU* mutants lost their ability to twitch in a typical agar stab assay, and have been reported as being hyperpiliated[21]. In *Neisseria gonorrhoeae*, PilU has no apparent role in twitching motility[22]. In our visualizations, while *pilT*⁻ *fliC*⁻ could not trigger retraction in the timescales of our visualizations, a *pilU*⁻ *fliC*⁻ deletion mutant could still transition to a tensed state, demonstrating its ability to retract TFP (Fig. 3a and Supplementary Videos 5 and 6). In addition, *pilU*⁻ *fliC*⁻ tends to have fewer, not more, TFP compared to *fliC*⁻, in contrast to *pilT*⁻ *fliC*⁻ (Fig. 3b and Supplementary Videos 5 and 6). Thus although cells lacking *pilU* can retract TFP, they do not migrate in typical twitching assays where colonies spread at the interface between a plastic dish and agar (Supplementary Fig. 5)[20]. We sought to elucidate this paradox by examining TFP dynamic activity. We first found that TFP length was identical between *fliC*, *pilU*⁻ *fliC*⁻ and *pilT*⁻ *fliC*⁻, demonstrating that extension is not affected (Fig. 3c). Although retraction frequency was slightly decreased in *pilU*⁻ *fliC*⁻ compared to *fliC*⁻ (Fig. 3d), this could not explain the total loss of motility observed in twitching assays. Finally, measurement of displacements in free solution on glass showed that each retraction generates an approximately similar displacement in *fliC*⁻ and *pilU*⁻ *fliC*⁻ (Fig. 3e and Supplementary Videos 2, 7). This demonstrated that TFP in cells lacking *pilU* do not lose their ability to generate displacements.

Since dynamics were not grossly affected by the absence of PilU in free solution, we sought to highlight a potential role of PilU in

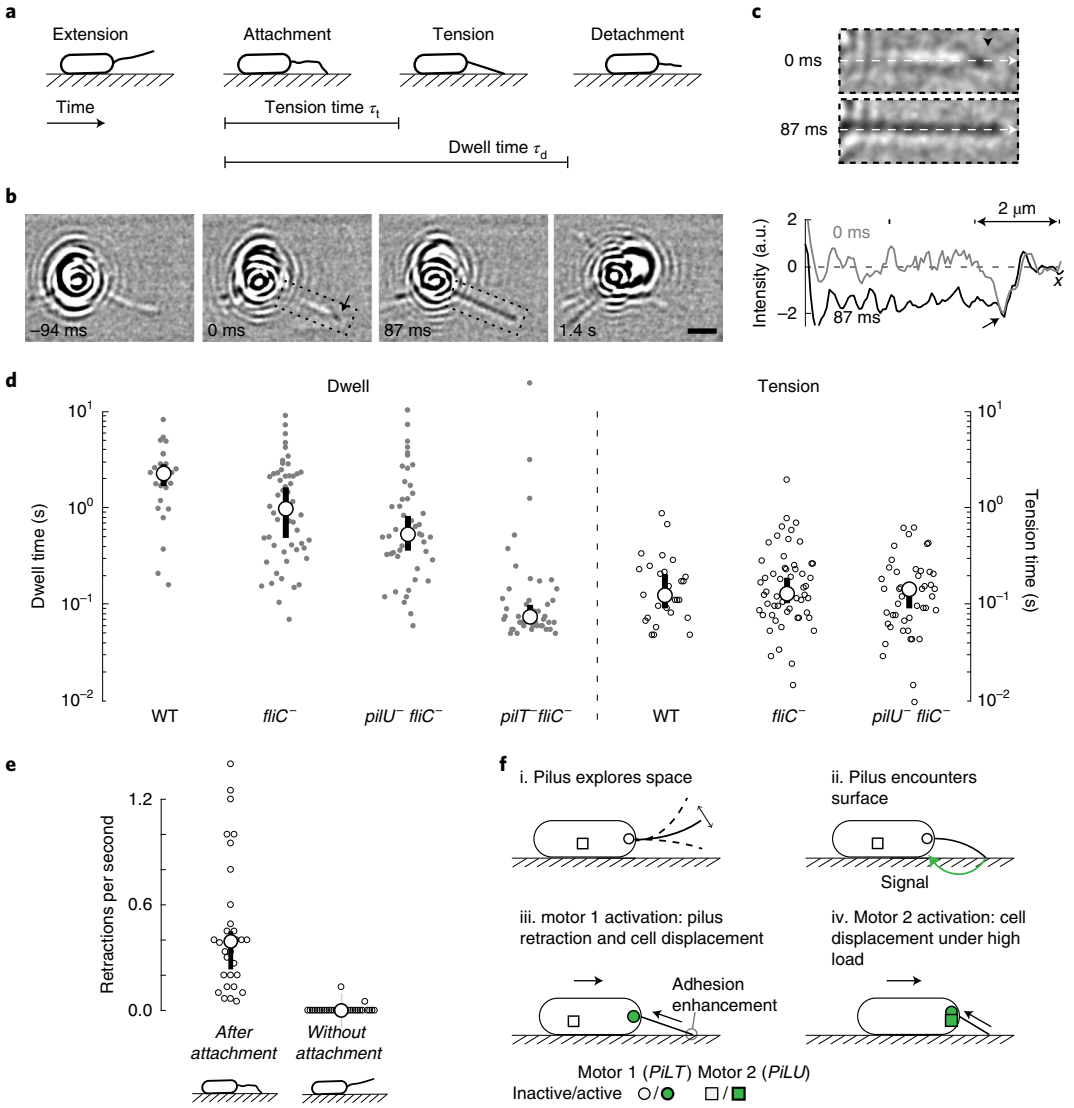

Fig. 4 | Coordination of TFP retraction motors. a, Illustration of the optimal sequence of events for TFP function: extension, attachment, tension and release from the surface. **b**, Successive events from **a** visualized with iSCAT. The attached pilus tip appears as a stationary dark signal at 0 ms (black arrow). The entire fibre transitions into lower-intensity values at $\tau_t = 87$ ms, before detaching at $\tau_d = 1.4$ s. Scale bar, 2 µm. **c**, Close-up view of attachment and tension from **b** with corresponding intensity profile along the pilus. A dip in intensity is observed at the tip at 0 ms (black arrow on image and graph), transitioning to a uniform low value at τ_t. **d**, Measurement of dwell and tension times in wild-type (WT) (total number of pili from at least three biological replicates, $n = 27$), *fliC*⁻ ($n = 54$), *pilU*⁻ *fliC*⁻ ($n = 47$) and *pilT*⁻ *fliC*⁻ ($n = 45$) cells. Comparison of retraction-capable and retraction-deficient mutants shows that TFP tension increased dwell time. The tension times in retraction-capable cells are close to the dwell time of *pilT*⁻ *fliC*⁻, showing that motors engage rapidly to initiate retraction. There is no defect in tension time in *pilU*⁻ *fliC*⁻, indicating that PilT is sufficient to initiate this rapid response. **e**, TFP retraction frequencies for attached and unattached TFP in *fliC*⁻ (cells from at least three biological replicates $n = 30$). TFP retract mostly only after their tips touch the surface, indicating that attachment stimulates retraction. **d**,**e**, Small circles correspond to individual measurements, large circles to median and error bars to bootstrap 95% confidence intervals. A difference between two groups is defined as statistically significant when their 95% confidence intervals do not overlap. **f**, Proposed model for sequential control of TFP motion. During spatial fluctuations (i), attachment of TFP tip to the surface generates a signal activating PilT (ii). This causes pilus retraction and tension, reinforcing attachment and resulting in longer dwell times and cell displacement (iii). PilU engages with power cell displacement under strong loads—for example, in environments with increased friction on the cell body (iv).

generating retraction force. We visualized twitching motility at the leading edge of colonies sandwiched between glass and agarose surfaces by phase contrast microscopy (we could not implement iSCAT because the gel scatters to a great extent). We reasoned that friction between the cell body and substrate during locomotion in this configuration is higher than in free solution, thus requiring greater forces to generate displacements during retraction. *fliC*⁻ cells at the leading edge of expanding twitching colonies were highly motile between glass and 0.5% agarose gel (Supplementary Video 8, top left). In this same configuration, *pilU*⁻ and *pilU*⁻ *fliC*⁻ were barely motile, consistent with twitching assays (Supplementary Video 8, bottom). We could repeat this defect in *fliC*⁻ by increasing the friction of the cell body with the surface using a higher agarose concentration, which requires a higher retraction force to generate similar displacement (Supplementary Video 8 (top right) and Supplementary Fig. 6). Taken together, this suggests that PilU contributes to increasing TFP retraction force in conjunction with PilT rather than acting as an independent retraction motor. By analogy

with the torque-dependent recruitment of flagellar motors, PilU could be activated when PilT reaches a threshold force[23], consistent with the fact that PilU localizes at the leading poles of twitching cells[24]. Alternatively, PilU could regulate PilT activity—for example, either through direct interaction or by mediating the function of minor pilins inserted in TFP[25]. In summary, *P. aeruginosa* uses one motor, PilT, to twitch in a low-friction environment but leverages the companion ATPase PilU to power displacements when friction increases.

A key question arising from these movies of a priori random attachment and detachment events is how *P. aeruginosa* orchestrates force generation to drive motility. To optimally generate displacements, cells must coordinate TFP retraction with attachment and detachment (Fig. 4a)[3]. Is this sequence actively coordinated or do TFP randomly extend and retract? To answer this, we performed visualizations of each step involved in individual TFP cycles (Fig. 4b and Supplementary Videos 9 and 10). We found that the tip of extended TFP occasionally appeared as a stationary dark spot while the remainder of the fibre fluctuated, indicating initial attachment. The same fibre then transitioned to a straight stationary line, indicating retraction and tension, before eventually detaching (Fig. 4c and Supplementary Videos 9 and 10). We could thus time the transitions between attachment, retraction and detachment of single fibres. We first measured the dwell time, τ_d, defined as the residence time of the pilus on the glass surface from tip attachment to detachment (Fig. 4a). The TFP of the retraction-less mutant *pilT*$^-$ *fliC*$^-$ could still attach, with a median dwell time of 75 ms (65–90 ms; median and 95% bootstrap confidence interval), which is a measurement of the intrinsic residence time of passive fibres on the surface (Fig. 4d). Given that the retraction speed of TFP is about 1 μm s^{-1}, this would enable only a seemingly short 70 nm displacement per retraction[13]. Surprisingly, the dwell time in cells capable of retraction was, however, much longer: 2,315 ms (1,710–2,635 ms) in wild-type, 997 ms (590–1,795 ms) in *fliC*$^-$ and 540 ms (405–840 ms) in *pilU*$^-$ *fliC*$^-$ (Fig. 4a). This indicates that tension force during retraction enhances TFP adhesion, increasing surface attachment time and thereby improving effective displacements of the cell body. In analogy with the formation of catch-bonds by the adhesin FimH in *Escherichia coli*, tension force may induce a conformational change in the structure of TFP, thereby increasing the strength of its attachment to the surface[26,27]. We also note that dwell times are typically less than 3 s, thereby facilitatinging TFP release for subsequent extension–retraction cycles, and that *pilU*$^-$ *fliC*$^-$ had slightly decreased dwell, possibly as a consequence of lower retraction strength.

The short dwell time of relaxed TFP on the surface suggests that retraction must take place rapidly after attachment. To achieve this, retraction must occur at high frequency or systematically after initial pilus contact with the surface. The first scenario would lead to inefficient conversion of force to displacement, while the second suggests that cells sense contact with their TFP. To identify the strategy used by *P. aeruginosa* to coordinate TFP retraction with attachment, we directly measured tension time, τ_t, defined as the delay between tip attachment and pilus tension (Fig. 4a). We found that TFP became tensed 130 ms (95–215 ms) after tip attachment in wild-type and 135 ms (105–198 ms) in *fliC*$^-$, which is close to the dwell time of relaxed TFP on the surface of *pilT*$^-$ *fliC*$^-$. Also, *pilU*$^-$ *fliC*$^-$ had a similar reactivity ($\tau_t = 150$ ms (90–155 ms)) (Fig. 4d), showing that PilT motors engage rapidly, optimizing retraction efficiency and subsequently increasing the dwell time of TFP on surfaces. This finding also hints at the possibility that cells sense tip attachment, which rapidly initiates retraction. Measuring the proportion of TFP retraction without attachment further supports this hypothesis: most extended TFP did not retract during the course of visualization unless their tip attached to the surface (Fig. 4e and Supplementary Fig. 7). This demonstrates that TFP attachment stimulates retraction, and that motors respond to a signal generated by contact of the tip with the surface. Thus, *P. aeruginosa* uses a high-efficiency sensing strategy to deploy and coordinate TFP rather than being reliant on random motor activation.

Our measurements indicate that *P. aeruginosa* precisely coordinates TFP motorized activity with attachment, by successively sensing surface contact, initiating retraction by a first motor, improving surface attachment during retraction through a catch-bond and triggering a second motor to generate displacement under high load (Fig. 4f). In the same manner as animal locomotion, the sequential control of pili movements could be coupled to sensory feedback enabling transformation into cell displacements, thereby increasing the efficiency of conversion of chemical energy into mechanical work. For example, animals use multiple sensory inputs such as mechano-sensation and proprioception to control and synchronize limb motion during locomotion[28,29]. Here, we suspect that tip contact generates a mechanical signal read by sensory components that triggers TFP retraction by PilT, and subsequent activation of PilU during twitching under high load. Combining visualizations of bacterial surface structure dynamics with molecular characterizations will eventually generate a holistic understanding of their functions, ultimately helping us to understand how microbes physically interact with their environment and highlighting shared strategies among seemingly distant living organisms[30].

Methods

Bacterial strains. Strains and plasmids used in this work were described previously[20]. Double-deletion mutant *pilTU*$^-$ *fliC*$^-$ was generated by conjugation of *pilTU*$^-$ mutants with the plasmid pJB215 using a standard mating protocol[31].

Glass coverslip preparation. Glass coverslips (22 × 40 mm^2 No. 1.5, Marienfeld) were cleaned as described in Young et al.[32]. Briefly, they were washed sequentially with distilled water, ethanol, distilled water, isopropanol, distilled water, ethanol and distilled water, with excess water removed by a stream of nitrogen. For visualization we used two platforms. In the first, we plasma-bonded polydimethylsiloxane (PDMS) micro-channels (width, 500 μm; depth, 90 μm) fabricated using standard photolithography methods. In the second platform, we deposited PDMS gaskets on clean coverslips. PDMS gaskets were obtained using biopsy punches of diameter 3 or 6 mm.

Sample preparation. Single colonies of the bacterial strains of interest were grown at 37 °C in Luria–Bertani medium overnight. Cultures were diluted 1:500 and grown to early exponential phase before visualization. For motility visualization, cells in early exponential phase were plated on plain Luria–Bertaniagar plates for 4 h, harvested by gentle flushing with Luria–Bertani medium followed by dilution to absorbance $A_{600} < 0.05$. The cells were loaded into either a microfluidic chip or PDMS gaskets. Micro-fluidic chips were first loaded with plain Luria–Bertani medium. After proper tubing, exhaust tubes were dipped in bacterial culture and cells were loaded by aspiration using a syringe pump (Crpump, No. ZS100). The gaskets were loaded with 20 μl of bacterial culture at $A_{600} < 0.05$ then washed twice with fresh Luria–Bertani after 5–10 min incubation at room temperature (if a higher A_{600} was used). When the loading process was complete, gaskets were sealed with a small coverslip to prevent liquid evaporation that would have generated fluctuations on iSCAT images.

We found that *fliC*$^-$ cells had more TFP compared to wild-type cells. We attribute this difference to our sample preparation process, which first selects for cells that reach and remain on the surface. This loading process induces positive selection for more piliated cells that attach more strongly to the coverslip.

Experimental set-up. Our experimental set-up is adapted from Ortega-Arroyo et al.[4] to allow live-cell visualization during long acquisition times (see schematic in Supplementary Fig. 1). We sought to reduce phototoxicity by using a laser wavelength of 635 nm for the iSCAT channel (Laserstack, No. LDM-638-700-C). The illumination beam was spatially filtered through a 50 μm pinhole and collimated with a 4*f* lens. The collimated beam was aligned into two perpendicular acousto-optic deflectors (AA Opto-Electronic, No. DTSXY-400-660) and imaged onto the back focal plane of the objective (Olympus, PLAN APO 60 × 1.42) using a 4*f* lens system, a polarizing beam splitter (Thorlabs, No. PBS251) and a quarter-wave plate (Thorlabs, No. AQWP05M-600). The acousto-optic deflectors allowed in-plane scanning of the beam on the sample. The objective captured the light scattered by the sample and the reflection of the incident beam at the glass–water interface. The quarter-wave plate and polarizing beam splitter discriminated input illumination from the reflected and scattered light. An achromatic lens (1,000 mm focal length) imaged the back focal plane of the objective onto a CMOS camera (PhotonFocus, No. MV1-D1024E-160-CL), yielding a 31.8 nm pixel size. Images

were acquired using LabView and a frame grabber (National Instruments, No. PCIe-1433). We added a mechanical shutter to the illumination path to prevent unnecessary illumination. We also implemented a brightfield channel by adding a white light-emitting diode (Thorlabs, No. WFA1010) above the stage and imaged the back focal plane of the objective on a CMOS camera (PointGrey, No. CM3-U3-31S4M) with an achromatic lens (focal length 400 mm, pixel size 25.9 nm). This brightfield channel allowed cell localization before iSCAT acquisition, thus protecting cells against extended light exposure.

Autofocus system. We ensured the *z*-position stability of our sample by building a cyto-compatible autofocus system with a weak infrared laser (850 nm, 3.5 mW; Thorlabs, No. CPS850). A CMOS camera (Thorlabs, No. DCC1545M) was used to detect total infrared light reflected by the glass–water interface, while LabView software computed drift correction providing real-time adjustment of the z-position of the stage through a piezo actuator.

Twitching motility assays. Motility assays were performed by stabbing and pipetting a 0.5% agarose Luria–Bertani plate with 2 µl of stationary-phase *P. aeruginosa* culture at the gel–plastic interface. The plates were incubated for 24 h at 30 °C before removal of agarose and staining of the plastic dish with a 0.1% solution of crystal violet in water. We performed microscopic twitching visualizations (Supplementary Video 8) by pipetting 0.5 µl of exponentially growing cells ($A = 0.1$ at 600 nm) on a 0.5% agarose Luria–Bertani pad. These were then flipped onto a glass-bottomed dish (Mattek, No. 1.5 coverslip) and incubated at 30 °C for 5 h. The leading edges of the expanding colonies were then visualized for 2 min at 1 frame s^{-1} by phase contrast microscopy on a Nikon TiE equipped with a×100, numerical aperture 1.45 objective and a Hamamatsu Orca R2 camera.

Image processing. To reveal the interferometric component of the signal, each frame of a given sequence was divided by a reference. This reference image was generated by computing the median of each pixel value throughout the entire stack of images. To improve visualization, we applied a band pass filter to dampen the contributions of small and large structures (smaller than 1 pixel and larger than 13 pixels) with the FFT plugin of ImageJ[33]. To reduce slight temporal variation in illumination, each frame was divided by its mean pixel gray value.

Image analysis of pili dynamics quantification. To extract time delays between attachment and retraction to a tensed state, we manually recorded the frame number of pili tip attachment (appearance of a stationary dark spot at the tip) and that of pili under tension (without pili fluctuations), where these events were clearly visible and could be measured with accuracy. Time delays were obtained by multiplying the frame difference by the acquisition frame time (frame rate, 200 frames s^{-1}). We measured tension times in 20 wild-type cells (27 retractions), 23 *liC*$^-$ cells (54 events) and 30 *pilU*$^-$ *fliC*$^-$ cells (47 events) from data acquired on a minimum of three separate days. Similarly, dwell times were obtained by manually measuring the time difference between attachment and detachment of each pilus from the same cells with the addition of 14 *pilT*$^-$ *fliC*$^-$ cells (45 events). Intensity measurement of attachment, tension and detachment was manually extracted by plotting the intensity profile along pili using plot profile, an ImageJ built-in tool. We performed intensity peak detection from the recorded profile for tip attachment, and tension using MatLab (Figs. 2 and 4). Pili length was measured from the tip attachment point to the middle of the first fringe of the cell body diffraction pattern from the same dataset. (Figs. 1 and 3). Retraction frequency was computed by counting all obvious retractions within a movie but discarding those pili already tensed in the initial frames. The total number of retractions was then divided by the movie time for 30 *fliC*$^-$ and 23 *pilU*$^-$ *fli*$^-$ cells (Fig. 3) from at least three biological replicates. Pili were counted on 20 wild-type, 15 *fliC*$^-$, 18 *fliC*$^-$ complemented, 19 *pilA*$^-$, 22 *pilA*$^-$ complemented, 11 *pilT*$^-$ *fliC*$^-$, 15 *pilT*$^-$ *fliC*$^-$ complemented, 18 *pilU*$^-$ *fliC*$^-$ and 17 *pilU*$^-$ *fliC*$^-$ complemented cells (Figs. 1 and 3) from the same strain culture. Flagella were counted from 52 wild-type, 51 *fliC*$^-$ and 50 *fliC*$^-$ complemented cells (Supplementary Fig. 2) from at least three biological replicates.

Image analysis of cell motility with iSCAT. Cell motility movies were acquired at 10 frames s^{-1} and binned ten times to obtain a final movie rate of 1 frame s^{-1}. The leading pole of the cell, defined as the centre of the white spot in the middle of the circular fringes of the cell body, was manually tracked during cell displacement (Supplementary Fig. 3). Only those cell displacements where no change in contrast of the leading pole was observed were recorded, to assess the effective influence of pili retraction on displacement and to discard Brownian motion effects when cells were not in contact with the glass surface. We note that some cells appeared to hover on the surface by Brownian motion, using TFP to maintain proximity to the surface. We recorded the number of visible retractions along each track. In total, 14 tracks were recorded for wild-type cells, 13 for *fliC*$^-$ and 15 for *pilU*$^-$ *fliC*$^-$ from the same strain culture (Fig. 3 and Supplementary Fig. 4).

Statistical analysis. As the time delay and tension time data were not normally distributed, we chose median as an indicator of the central tendency of distribution. Statistical analysis was performed using the bootstrap method in MatLab to resample the data of each strain into 300 different groups; and to compute the median of the medians of each bootstrap group, to obtain a more robust estimate of population behavior. We computed the 95% confidence interval by taking the highest and lowest values of the bootstrap median dataset after removing the top and bottom 2.5% of the data points. The same approach was used to determine retraction frequency, pili length and displacement per retraction. Pili numbers in complementation analysis were computed by taking the mean of the bootstrap medians and the bootstrap 95% confidence interval as stated previously. A difference between the two groups was defined as statistically significant when their 95% confidence intervals did not overlap.

Reporting Summary. Further information on research design is available in the Nature Research Reporting Summary linked to this article.

Code availability

All codes are available from the corresponding author upon reasonable request.

Data availability

All data are available from the corresponding author upon reasonable request.

Received: 13 August 2018; Accepted: 18 January 2019;
Published online: 25 February 2019

References

1. Gibiansky, M. L. et al. Bacteria use type iv pili to walk upright and detach from surfaces. *Science* **330**, 197 (2010).
2. Mattick, J. S. Type IV pili and twitching motility. *Annu. Rev. Microbiol.* **56**, 289–314 (2002).
3. Chang, Y. W. et al. Architecture of the type IVa pilus machine. *Science* **351**, aad2001 (2016).
4. Ortega-Arroyo, J., Cole, D. & Kukura, P. Interferometric scattering microscopy and its combination with single-molecule fluorescence imaging. *Nat. Protoc.* **11**, 617–633 (2016).
5. Costa, T. R. D. et al. Secretion systems in Gram-negative bacteria: structural and mechanistic insights. *Nat. Rev. Microbiol.* **13**, 343–359 (2015).
6. Persat, A. Bacterial mechanotransduction. *Curr. Opin. Microbiol.* **36**, 1–6 (2017).
7. Burrows, L. L. *Pseudomonas aeruginosa* twitching motility: type IV pili in action. *Annu. Rev. Microbiol.* **66**, 493–520 (2012).
8. Persat, A., Inclan, Y. F., Engel, J. N., Stone, H. A. & Gitai, Z. Type IV pili mechanochemically regulate virulence factors in *Pseudomonas aeruginosa*. *Proc. Natl Acad. Sci. USA* **112**, 7563–7568 (2015).
9. Merz, A. J., So, M. & Sheetz, M. P. Pilus retraction powers bacterial twitching motility. *Nature* **407**, 98–102 (2000).
10. Maier, B., Potter, L., So, M., Seifert, H. S. & Sheetz, M. P. Single pilus motor forces exceed 100 pN. *Proc. Natl Acad. Sci. USA* **99**, 16012–16017 (2002).
11. Beaussart, A. et al. Nanoscale adhesion forces of *Pseudomonas aeruginosa* type IV pili. *ACS Nano.* **8**, 10723–10733 (2014).
12. Jin, F., Conrad, J. C., Gibiansky, M. L. & Wong, G. C. L. Bacteria use type-IV pili to slingshot on surfaces. *Proc. Natl Acad. Sci. USA* **108**, 12617–12622 (2011).
13. Skerker, J. M. & Berg, H. C. Direct observation of extension and retraction of type IV pili. *Proc. Natl Acad. Sci. USA* **98**, 6901–6904 (2001).
14. Ellison, C. K. et al. Obstruction of pilus retraction stimulates bacterial surface sensing. *Science* **358**, 535–538 (2017).
15. Ortega Arroyo, J. et al. Label-free, all-optical detection, imaging, and tracking of a single protein. *Nano. Lett.* **14**, 2065–2070 (2014).
16. Kukura, P. et al. High-speed nanoscopic tracking of the position and orientation of a single virus. *Nat. Methods* **6**, 923–927 (2009).
17. Ping, L., Birkenbeil, J. & Monajembashi, S. Swimming behavior of the monotrichous bacterium *Pseudomonas fluorescens* SBW25. *FEMS Microbiol. Ecol.* **86**, 36–44 (2013).
18. Ortega-Arroyo, J. & Kukura, P. Interferometric scattering microscopy (iSCAT): new frontiers in ultrafast and ultrasensitive optical microscopy. *Phys. Chem. Chem. Phys.* **14**, 15625 (2012).
19. Krishnan, M., Mojarad, N., Kukura, P. & Sandoghdar, V. Geometry-induced electrostatic trapping of nanometric objects in a fluid. *Nature* **467**, 692–695 (2010).
20. Bertrand, J. J., West, J. T. & Engel, J. N. Genetic analysis of the regulation of type IV pilus function by the Chp chemosensory system of *Pseudomonas aeruginosa*. *J. Bacteriol.* **192**, 994–1010 (2010).
21. Whitchurch, C. B. & Mattick, J. S. Characterization of a gene, pilU, required for twitching motility but not phage sensitivity in *Pseudomonas aeruginosa*. *Mol. Microbiol.* **13**, 1079–1091 (1994).
22. Park, H.-S. M., Wolfgang, M. & Koomey, M. Modification of Type IV pilus-associated epithelial cell adherence and multicellular behavior by the pilu protein of *Neisseria gonorrhoeae*. *Infect. Immun.* **70**, 3891–3903 (2002).

23. Kuchma, S. L. et al. Cyclic Di-GMP-mediated repression of swarming motility by *Pseudomonas aeruginosa* PA14 requires the MotAB stator. *J. Bacteriol.* **197**, 420–430 (2015).
24. Chiang, P., Habash, M. & Burrows, L. L. Disparate subcellular localization patterns of *Pseudomonas aeruginosa* type iv pilus atpases involved in twitching motility. *J. Bacteriol.* **187**, 829–839 (2005).
25. Giltner, C. L., Nguyen, Y. & Burrows, L. L. Type IV pilin proteins: versatile molecular modules. *Microbiol. Mol. Biol. Rev.* **76**, 740–772 (2012).
26. Thomas, W. E., Vogel, V. & Sokurenko, E. Biophysics of catch bonds. *Annu. Rev. Biophys.* **37**, 399–416 (2008).
27. Biais, N., Higashi, D. L., Brujic, J., So, M. & Sheetz, M. P. Force-dependent polymorphism in type IV pili reveals hidden epitopes. *Proc. Natl Acad. Sci. USA* **107**, 11358–11363 (2010).
28. Kiehn, O. Decoding the organization of spinal circuits that control locomotion. *Nat. Rev. Neurosci.* **17**, 224–238 (2016).
29. Dietz, V. Proprioception and locomotor disorders. *Nat. Rev. Neurosci.* **3**, 781–790 (2002).
30. Persat, A. et al. The mechanical world of bacteria. *Cell* **161**, 988–997 (2015).
31. Hmelo, L. R. et al. Precision-engineering the *Pseudomonas aeruginosa* genome with two-step allelic exchange. *Nat. Protoc.* **10**, 1820–41 (2015).
32. Young, G. et al. Quantitative mass imaging of single biological macromolecules. *Science* **360**, 423–427 (2018).
33. Schindelin, J. et al. Fiji: an open-source platform for biological-image analysis. *Nat. Methods* **9**, 676–682 (2012).

Acknowledgements

The authors would like to thank J. Andrecka for valuable discussions on iSCAT, J. Engel and Y. Inclan for strains and plasmids and Z. Al-Mayyah for help with generating one mutant strain. L.T. and A.P. thank the Swiss National Foundation for funding this work through Projects (grant No. 31003A_169377) and the Gabriella Giorgi-Cavaglieri Foundation.

Author contributions

L.T. and A.P conceptualized the study and performed experiments and data analysis. L.T., A.F. and P.K. implemented and adapted the iSCAT microscope for live-cell imaging. L.T., P.K and A.P. wrote the manuscript.

Competing interests

The authors declare no competing interests.

Additional information

Supplementary information is available for this paper at https://doi.org/10.1038/s41564-019-0378-9.

Reprints and permissions information is available at www.nature.com/reprints.

Correspondence and requests for materials should be addressed to A.P.

Publisher's note: Springer Nature remains neutral with regard to jurisdictional claims in published maps and institutional affiliations.

nature research

Corresponding author(s): Alexandre Persat

Reporting Summary

Nature Research wishes to improve the reproducibility of the work that we publish. This form provides structure for consistency and transparency in reporting. For further information on Nature Research policies, see Authors & Referees and the Editorial Policy Checklist.

Statistical parameters

When statistical analyses are reported, confirm that the following items are present in the relevant location (e.g. figure legend, table legend, main text, or Methods section).

n/a	Confirmed	
☐	☒	The exact sample size (*n*) for each experimental group/condition, given as a discrete number and unit of measurement
☐	☒	An indication of whether measurements were taken from distinct samples or whether the same sample was measured repeatedly
☒	☐	The statistical test(s) used AND whether they are one- or two-sided *Only common tests should be described solely by name; describe more complex techniques in the Methods section.*
☒	☐	A description of all covariates tested
☐	☒	A description of any assumptions or corrections, such as tests of normality and adjustment for multiple comparisons
☐	☒	A full description of the statistics including central tendency (e.g. means) or other basic estimates (e.g. regression coefficient) AND variation (e.g. standard deviation) or associated estimates of uncertainty (e.g. confidence intervals)
☒	☐	For null hypothesis testing, the test statistic (e.g. *F*, *t*, *r*) with confidence intervals, effect sizes, degrees of freedom and *P* value noted *Give P values as exact values whenever suitable.*
☒	☐	For Bayesian analysis, information on the choice of priors and Markov chain Monte Carlo settings
☒	☐	For hierarchical and complex designs, identification of the appropriate level for tests and full reporting of outcomes
☒	☐	Estimates of effect sizes (e.g. Cohen's *d*, Pearson's *r*), indicating how they were calculated
☐	☒	Clearly defined error bars *State explicitly what error bars represent (e.g. SD, SE, CI)*

Our web collection on statistics for biologists may be useful.

Software and code

Policy information about availability of computer code

Data collection	Images were acquired using LabVIEW 2016, version 16.0f5 (64-bit).
Data analysis	Images were processed and quantified using ImageJ, version 1.51n. Bootstrap analysis was made using MatLab version R2016b (9.1.0.441655).

For manuscripts utilizing custom algorithms or software that are central to the research but not yet described in published literature, software must be made available to editors/reviewers upon request. We strongly encourage code deposition in a community repository (e.g. GitHub). See the Nature Research guidelines for submitting code & software for further information.

Data

Policy information about availability of data

All manuscripts must include a data availability statement. This statement should provide the following information, where applicable:

- Accession codes, unique identifiers, or web links for publicly available datasets
- A list of figures that have associated raw data
- A description of any restrictions on data availability

All data are available from the corresponding author upon reasonable request.

Field-specific reporting

Please select the best fit for your research. If you are not sure, read the appropriate sections before making your selection.

☒ Life sciences ☐ Behavioural & social sciences ☐ Ecological, evolutionary & environmental sciences

For a reference copy of the document with all sections, see nature.com/authors/policies/ReportingSummary-flat.pdf

Life sciences study design

All studies must disclose on these points even when the disclosure is negative.

Sample size	We did not have initial guesses for absolute and relative values of time delays (Fig. 4d). We therefore used intermediate sample size (N for pili measured >20) and performed statistical analysis without any assumption on the underlying distribution (using the bootstrap method). Measurements of retraction events were more difficult and based on rare events, in particular for unattached pili (Fig. 4e). However our initial observations hinted that the effect would be dramatic between unattached vs attached, we thus settled for measuring events from 30 fliC- cells and 23 pilU- fliC- cells. We incresed our sample size by at least 2 compared to our first submission.
Data exclusions	Due to the sensitivity of the technique we decided to discarded movies that were of bad quality (too much background noise, out of focus acquisition, floating cells, etc) prior to data acquisition as such movies didn't allow proper pili detection and image analysis. In order to study the effect of pili retraction on cell body motility while attaching on surfaces we decided to discard movies were cells moved by hopping movements with only short residence time.
Replication	Measurements for pili length, retraction frequencies, dwell time and tension time were performed in at least 3 biological replicates. Pili number from each strain and corresponding complementation strains were counted on several cells from a same strain culture. Motility measurements were extracted from several tracks from a same strain culture.
Randomization	Cells were visualized in bright-field and were randomly selected prior to visualization with iSCAT.
Blinding	Blinding was not possible as the experimenter performed both the acquisition and Image analysis.

Reporting for specific materials, systems and methods

Materials & experimental systems

n/a	Involved in the study
☐	☒ Unique biological materials
☒	☐ Antibodies
☒	☐ Eukaryotic cell lines
☒	☐ Palaeontology
☒	☐ Animals and other organisms
☒	☐ Human research participants

Methods

n/a	Involved in the study
☒	☐ ChIP-seq
☒	☐ Flow cytometry
☒	☐ MRI-based neuroimaging

Unique biological materials

Policy information about availability of materials

Obtaining unique materials	All strains and plasmids described in this manuscript were previously described in Bertrand et al. J. Bacteriol. 2010 and are available upon request.